universe

MDPI

Article

Tachyon Condensation in a Chromomagnetic Center Vortex Background

Michael Bordag

Bogoljubov Laboratory of Theoretical Physics, Joint Institute for Nuclear Research, 141980 Dubna, Russia; bordag@mail.ru

Abstract: The chromomagnetic vacuum of SU(2) gluodynamics is considered in the background of a finite radius flux tube (center vortex) with a homogeneous field inside and a zero field outside. In this background, there are tachyonic modes. These modes cause an instability. It is assumed that the self-interaction of these modes stops the creation of gluons, and it is assumed that a condensate will be formed. For constant condensates, the minimum of the effective potential is found at the tree level. In the background of these condensates, all tachyonic modes acquire non-zero real masses, which will result in a real effective potential of this system. Considering only the tachyonic modes and adding the energy of the background field, the total energy is found to have a minimum at some value of the background field, which depends on the coupling of the initial SU(2) model. For small coupling, this dependence is polynomial in distinction from the Savvidy vacuum where it is exponentially suppressed. The minimum of this energy will deepen with a shrinking radius of the flux tube. It can be expected that this process can be stopped by adding quantum effects. Using the high-temperature expansion of the effective potential, it can be expected that the symmetry, which is broken by the condensate, will be restored at sufficiently high temperatures.

Keywords: QCD; vacuum; tachyonic mode; color magnetic field; effective potential

Citation: Bordag, M. Tachyon Condensation in a Chromomagnetic Center Vortex Background. *Universe* **2024**, *10*, 38. https://doi.org/10.3390/universe10010038

Academic Editor: Santiago Peris

Received: 4 December 2023
Revised: 8 January 2024
Accepted: 10 January 2024
Published: 12 January 2024

1. Introduction

Quantum chromodynamics (QCD) is the quantum field theory that describes the strong interactions. It is renormalizable and, thanks to its asymptotic freedom, it is successful in the high-energy region, wherein a perturbative treatment is possible. In distinction, in the low-energy region, one hits infrared problems originating from the masslessness of the gluon fields. Physically, one observes confinement, which is probably due to a strong multiparticle interaction of gluons and quarks. In addition, and in distinction from QED, the basic fields of QCD do not correspond to the asymptotic states of the theory.

The confinement of gluons and quarks is the main problem left open in the Standard Model. There were many approaches and attempts to solve it. Especially, lattice calculations give a strong support for the idea of confinement and provide good suggestions for responsible field configurations, the most convincing one being the dual superconductor configuration. Another approach rests on the functional renormalization group (FRG) by solving flow equations towards some fixed point; see [1], for example. A common feature of these approaches is to look for a condensate of gluons that could solve the infrared problems caused by their masslessness, thereby keeping the gauge invariance.

A completely different approach rests on the observation that the magnetic moment of the gluons—due to their spin one, which is twice that of the electron—overcompensates the lowest Landau level in a chromomagnetic field. In a (homogeneous) field B, the one particle energy of a gluon,

$$E_n = \sqrt{p_z^2 + gB(2n + 1 + 2s)}, \tag{1}$$

may become imaginary in the lowest state ($n = 0$ and $s = -1$). Such a state is called *tachyonic*. If considering the effective potential, or equivalently, the first quantum corrections to the classical ground state, one arrives at the formula

$$V_{eff} = \frac{B^2}{2} + \frac{11B^2}{48\pi^2} \ln \frac{gB}{\mu} + i\frac{(gB)^2}{8\pi}, \tag{2}$$

where μ is a normalization constant. As first observed in [2], there is a minimum at some finite B where $V_{eff} < 0$, causing the spontaneous generation of such field and forming a new ground state (chromomagnetic or Savvidy vacuum). The reason behind this is the coefficient in front of the logarithm, which is the first coefficient in the beta function, and its sign is that of asymptotic freedom. However, in [3], the imaginary part in (2) was observed, which makes this vacuum state unstable.

There were many attempts to overcome the instability of the chromomagnetic vacuum state. The first one was the so-called *Copenhagen vacuum*; see [4]. It rests on the observation that the instability for its formation needs a certain spatial region of a slowly varying background field for instance to have $gB < p_3^2$ in (1). One expects a certain domain structure to be formed. Also, in [5], attention was paid to the observation that the instability occurs from the quadratic part of the action and that the tachyonic modes have a nonlinear, ϕ^4-type self-interaction, which acts repulsive. Another approach starts from a self-dual background. In such a background that necessarily also involves a chromoelectric field, the effective potential also has a minimum like (2) but without the imaginary part. In the place, one has an infinite number of zero modes [6]. Also, the formulation is in a Euclidean space and is returning to Minkowski space, and the electric field becomes imaginary.

Recently, ref. [7] was able to sum up these zero modes. Furthermore, it was shown there that the electric field may be switched off while keeping the imaginary part away. As a result, Equation (2) without the imaginary part was obtained. A similar result was obtained in [8], where the gluon polarization tensor was accounted for in some approximations.

It must be mentioned that the Savvidy vacuum has two more unwanted features. The minimum in (2) appears for $gB = \mu^2 \exp\left(-\frac{24\pi^2}{11g^2}\right)$, i.e., it is exponentially small in a perturbative region. Furthermore, as shown in [9], the symmetry breaking caused by the chromomagnetic vacuum state is not restored at high temperature.

The masslessness of the gluon, which is a necessary feature for the gauge symmetry, hampers all attempts for perturbative calculations in the low-energy region. There have been many attempts to introduce a mass. As an example, we mention [10], where a special source term was introduced using the formalism of local composite operators introduced by the authors earlier together with a chromomagnetic background field. However, removing the source, which acts like a gluon mass, brings the instability back.

A decade ago, in [1], which used the functional renormalization group approach with a self-dual background field, an effective potential like (2) without the imaginary part was found, but with physically more realistic parameters. In [11], using a complex flow equation, a minimum of the effective potential was found, first without a magnetic background field. When switching on the magnetic field, the imaginary part re-appeared.

Quite recently, the idea of a domain structure was put forward in [12] (and citations therein). The domains are assumed to be filled by a self-dual background. The emerging quasi-normal modes are treated beyond one loop, and the competition between the energy of the domains and the disorder was considered. By minimizing the overall free energy, a finite size for the domains was demonstrated. However, it must be mentioned that all such attempts were unsatisfactory so far.

An attempt to extend the chromomagnetic vacuum from a homogeneous background to a string-like configuration was undertaken in [13]. There, for a cylindrical chromomagnetic background field with several profile functions decreasing at infinity, thus having a finite flux and a finite energy (per unit length in direction of the cylinder), the effective potential was calculated. Such configurations show a vacuum energy similar to (2), i.e.,

some non-trivial minimum. However, in [13], no tachyonic mode was seen; however, it should be there, as shown in [14].

In [15], as a new idea for the instability problem, it was suggested to consider a Higgs mechanism for the unstable mode. This mode, as defined by $n = 0$ and $s = -1$ in (1), is a complex field in two dimensions (x_α, $\alpha = 0, 3$), where x_3 is the direction of the magnetic background field with a negative mass square,

$$m^2 = -gB < 0. \tag{3}$$

In such a state, due to the instability, gluon pairs will be created. These are bosons and will form a condensate of tachyons until the process is stopped by their repulsive self-interaction. Technically, the potential in the corresponding Lagrangian has a 'Mexican hat' shape, and it is necessary to use the Higgs mechanism by making a shift of the tachyon field and quantizing around the shifted field. This was performed in [15] for a homogeneous background in a radial gauge. Restricting to the lowest orbital mode ($l = 0$), one comes to a model with a single complex field in two dimensions. Application of the second Legendre transform in Hartree approximation (or the CJT formalism) resulted in an effective potential with a minimum as a function of the background field that was below zero at perturbative values of the parameters (in distinction from (2), where the minimum for small coupling is exponentially small). Raising the temperature lifted this minimum until it disappeared after a certain critical temperature. In this way, the symmetry, which was broken by the condensate, is restored.

The paper [15] has several shortcomings. First of all, a homogeneous background field is not really physical but an approximation at best. Second, the restriction to the lowest orbital momentum mode needs a better justification. Finally, within the given approach, a phase transition in a two-dimensional system was seen, which seems to be in contradiction with the Mermin–Wagner theorem.

In the present paper, I will solve some of the mentioned problems. I consider as a background a finite-radius chromomagnetic magnetic flux tube and consider all appearing orbital momentum modes of the tachyonic field. Such a background is a special case of a center vortex background, which is frequently discussed in connection with the confinement problem.

The paper is organized as follows. In Section 2, the basic formulas for SU(2) are introduced. In Section 3, I define the background and tachyonic mode and derive the corresponding two-dimensional Lagrangian. Section 4 is devoted to the tachyon condensate and to finding the minimum of the energy. Afterwards is the conclusion. A technical part is delegated to the Appendix A.

In this paper, I use units with $c = \hbar = 1$.

2. Basic Formulas

We consider SU(2) gluodynamics in Euclidean space with the Lagrangian

$$\mathcal{L} = \mathcal{L}_{\rm YM} + \mathcal{L}_{\rm gf} + \mathcal{L}_{\rm gh} \tag{4}$$

where

$$\begin{aligned} \mathcal{L}_{\rm YM} &= -\frac{1}{4}\Big(F^a_{\mu\nu}[A]\Big)^2, \\ \mathcal{L}_{\rm gf} &= -\frac{1}{2\xi}\Big(D^{ab}_\mu Q^b_\mu\Big)(D^{ac}_\nu Q^c_\nu), \\ \mathcal{L}_{\rm gh} &= \bar{c}^a\Big(-D^{ac}_\mu D^{cb}_\mu - gD^{ac}_\mu \epsilon^{cdb} Q^d_\mu\Big)c^b, \end{aligned} \tag{5}$$

are the Yang–Mills Lagrangian, the gauge fixing term (in background gauge), and the ghost contribution. The field strengths are

$$F^a_{\mu\nu}[A] = \partial_\mu A^a_\nu - \partial_\nu A^a_\mu + g\epsilon^{abc} A^b_\mu A^c_\nu. \tag{6}$$

A background field B^a_μ is introduced by

$$A^a_\mu = B^a_\mu + Q^a_\mu, \tag{7}$$

where Q^a_μ is the quantum field. The field strength (6) turns into

$$F^a_{\mu\nu}[B+Q] = F^a_{\mu\nu}[B] + D^{ab}_\mu Q^b_\nu - D^{ab}_\nu Q^b_\mu + g\epsilon^{abc} Q^b_\mu Q^c_\nu \tag{8}$$

with the covariant derivative

$$D^{ab}_\mu = \partial_\mu \delta^{ab} + g\epsilon^{acb} B^c_\mu. \tag{9}$$

We mention its commutator,

$$\left[D_\mu, D_\nu\right]^{ab} = g\epsilon^{acb} F^c_{\mu\nu}[B]. \tag{10}$$

With the background field B^a_μ, introduced in (7), the gauge fixing Lagrangian $\mathcal{L}_{\rm gf}$ in (6) defines an R_ξ gauge. In the following, we put $\xi = 1$, i.e., we work in the Feynman gauge. We mention that when not going beyond the one-loop approximation in the effective action, the gauge invariance should be guaranteed.

We insert (8) into (5),

$$\mathcal{L}_{\rm YM} = \mathcal{L}_0 + \mathcal{L}_1 + \mathcal{L}_2 + \mathcal{L}_3 + \mathcal{L}_4, \tag{11}$$

where

$$\mathcal{L}_0 = -\frac{1}{4}\Big(F^a_{\mu\nu}[B]\Big)^2 \tag{12}$$

is the (classical) background contribution,

$$\mathcal{L}_1 = Q^a_\nu D^{ab}_\mu B^b_{\mu\nu} \tag{13}$$

with $B^b_{\mu\nu} = \partial_\mu B^b_\nu - \partial_\nu B^b_\mu$ being the linear term (source term), and the remaining contributions

$$\begin{aligned}
\mathcal{L}_2 &= -\frac{1}{2} Q^a_\mu \Big(-(D^a_\lambda)^2 \delta_{\mu\nu} - 2g\epsilon^{acb} B^c_{\mu\nu} \Big) Q^b_\nu, \\
\mathcal{L}_3 &= -g\epsilon^{abc} (D^{ad}_\mu Q^d_\nu) Q^b_\mu Q^c_\nu, \\
\mathcal{L}_4 &= -\frac{g^2}{4} (Q^a_\mu Q^a_\mu Q^b_\nu Q^b_\nu - Q^a_\mu Q^a_\nu Q^b_\mu Q^b_\nu).
\end{aligned} \tag{14}$$

are quadratic, cubic, and quartic in the quantum field.

In the following, we consider an Abelian background field

$$B^a_\mu = \delta^{a3} B_\mu, \quad B_{\mu\nu} = \partial_\mu B_\nu - \partial_\nu B_\mu. \tag{15}$$

With this, it is convenient to turn into the so-called *charged basis*, which diagonalizes the Lagrangian in color space. By performing the corresponding substitutions,

$$Q^1_\mu = \frac{1}{\sqrt{2}}(W_\mu + W^*_\mu), \qquad Q^3_\mu = Q_\mu, \tag{16}$$
$$Q^2_\mu = \frac{1}{\sqrt{2}i}(W_\mu - W^*_\mu), \qquad W_\mu = \frac{1}{\sqrt{2}}\Big(Q^1_\mu + iQ^2_\mu\Big).$$

in (14), we arrive at

$$\begin{aligned}\mathcal{L}_2 &= -\frac{1}{2}Q_\mu\Big(-\partial^2\delta_{\mu\nu}\Big)Q_\nu \\ &\quad - W^*_\mu\Big(-(D_\lambda)^2\delta_{\mu\nu} - 2igB_{\mu\nu}\Big)W_\nu, \\ \mathcal{L}_3 &= -ig(Q_\mu W^*_{\mu\nu}W_\nu - Q_\mu W_{\mu\nu}W^*_\nu - Q_{\mu\nu}W^*_\mu W_\nu) \\ \mathcal{L}_4 &= -g^2(Q_\mu Q_\mu W^*_\nu W_\nu - Q_\mu Q_\nu W^*_\mu W_\nu \\ &\quad + W^*_\mu W_\mu W^*_\nu W_\nu - W^*_\mu W_\nu W^*_\mu W_\nu).\end{aligned} \tag{17}$$

The third component, Q_μ, is interpreted as a color-neutral vector field, whereas W_μ represents a color-charged vector field. In (17), we introduced the notations

$$Q_{\mu\nu} = \partial_\mu Q_\nu - \partial_\nu Q_\mu, \;\; W_{\mu\nu} = D_\mu W_\nu - D_\nu W_\mu, \tag{18}$$

and the covariant derivative for the charged field is

$$D_\mu = \partial_\mu - iB_\mu, \quad [D_\mu, D_\nu] = -iB_{\mu\nu}. \tag{19}$$

In the following section, we specialize these general formulas to the case of a cylindrical symmetric background field.

3. Cylindrically Symmetric Background Field and a Field Theory for the Tachyonic Mode

We consider a cylindrical symmetric chromomagnetic magnetic background field, for instance, a straight vortex line parallel to the third spatial axis. In cylindrical coordinates (r, φ, x_3), we take the upper two components of the potential B_μ, $\mu = 1, 2$, in the form (in two-dimensional vector notations)

$$\vec{B} = \vec{e}_\varphi \frac{\mu(r)}{r}, \tag{20}$$

together with $B_3 = B_4 = 0$. The radial profile $\rho(r)$ is, for the moment, arbitrary. The field strengths in (15) turn into

$$B_{\mu\nu} = \epsilon_{\mu\nu}\frac{\mu'(r)}{r}, \quad \epsilon_{\mu\nu} = \begin{pmatrix} 0 & 1 & 0 & 0 \\ -1 & 0 & 0 & 0 \\ 0 & 0 & 0 & 0 \\ 0 & 0 & 0 & 0 \end{pmatrix}_{\mu\nu} \tag{21}$$

and for the commutator, we obtain

$$[D_1, D_2] = -i\,\frac{\mu'(r)}{r}. \tag{22}$$

We mention that in our notations, B_μ in (14) is the potential and $B_{\mu\nu}$ is the field strength of the background field. In (21),

$$\frac{\mu'(r)}{r} \equiv B(r), \tag{23}$$

has the meaning of the modulus of the three-dimensional field strength belonging to the vector potential (20).

Next, we consider the linear term (13). With (9) and (13), we obtain

$$\mathcal{L}_1 = Q^3_\nu \partial_\mu \epsilon_{\mu\nu} \frac{\mu'(r)}{r} \tag{24}$$

and using (21), we arrive at

$$\mathcal{L}_1 = (-\sin\varphi Q^3_1 + \cos\varphi Q^3_2)\left(\frac{\mu'(r)}{r}\right)'. \tag{25}$$

In a homogeneous background field where $B(r) = const$ in (23), $\mathcal{L}_1$ vanishes. In a non-homogeneous background, which we will consider below, it does not vanish. However, it couples to the third color component, i.e., to the color-neutral one, which does not influence the tachyonic mode.

Next, we define the tachyonic mode. We consider the spectrum of the operator representing the kernel of the quadratic part in W_μ, $\mathcal{L}_2$ in (17). The corresponding wave equation reads

$$\Big((D_\lambda)^2\delta_{\mu\nu} - 2igB_{\mu\nu}\Big)W_\nu = 0. \tag{26}$$

In a homogeneous background, we have a profile function

$$\mu(r) = \frac{Br^2}{2}, \quad \frac{\mu'(r)}{r} = B, \tag{27}$$

with a constant B and, after Fourier transform in the time and z-directions, the spectrum is well known,

$$k_0^2 = k_3^2 + gB(2n + 1 + 2s), \tag{28}$$

where $n = 0, 1, \ldots$ enumerates the Landau levels and $s = \pm 1$ is the spin projection. The tachyonic mode is defined by $n = 0$, $s = -1$, and its spectrum,

$$k_0^2 = k_3^2 - gB, \tag{29}$$

has a negative eigenvalue, which can be interpreted as a negative mass square, $m^2 = -gB$. As mentioned in the Introduction, this is the reason we call it tachyonic. Also, it is frequently called *the unstable mode.* In fact, this is not a single mode. In the eigenvalue problem (26), there is a further quantum number, the orbital momentum, with respect to which the spectrum is degenerated. This corresponds to the translational invariance of the problem in the plane perpendicular to the magnetic field. In this sense, there are infinitely many tachyonic modes.

In the present paper, we consider a magnetic field that is homogeneous inside a cylinder of radius R and zero outside. In this case, the profile function is

$$\mu(r) = \frac{Br^2}{2}\Theta(R - r) + \frac{BR^2}{2}\Theta(r - R), \quad \frac{\mu'(r)}{r} \equiv B(r) = B\,\Theta(R - r), \tag{30}$$

This field has a finite flux, Φ, and a finite energy, E_{bg},

$$\Phi = \int d^2x_\perp B(r) = \pi R^2 B, \quad E_{bg} = \frac{1}{2}\int d^2x_\perp B(r)^2 = \frac{\pi}{2}B^2R^2, \tag{31}$$

the energy being a density per unit lengths of the third direction. In this background, the spectrum of the color-charged field W_μ, (16), is more complicated then (29). Nevertheless, it has tachyonic modes,

$$k_0^2 = k_3^3 - \kappa_l^2, \tag{32}$$

with $\kappa_l^2 > 0$; see Figure 1.

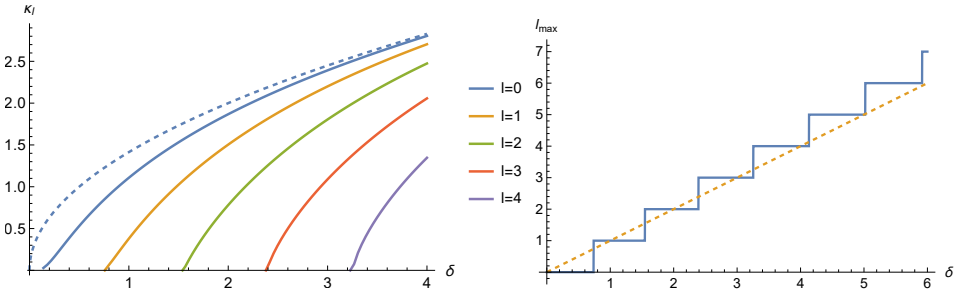

Figure 1. Left panel: The tachyonic levels (32) in the flux tube (33). **Right panel**: The maximal number l_{max} of orbital momenta for a given flux δ (solid line). This is the number of curves crossed by a vertical section in the left panel. For comparison, the dashed line shows δ.

In this background, for the tachyonic modes $W_\mu^{\rm ta}(x)$, we consider the mode decomposition

$$W_\mu^{\rm ta}(x) = \frac{1}{\sqrt{2}} \begin{pmatrix} 1 \\ i \\ 0 \\ 0 \end{pmatrix}_\mu \sum_{l=0}^{l_{max}} \frac{e^{il\varphi}}{\sqrt{2\pi}} \phi_l(r)\psi_l(x_\alpha), \quad (\alpha = 0,3) \quad x_\perp = (r,\varphi), \tag{33}$$

($x_\perp$ taken in cylindrical coordinates), and l_{max} is discussed below. In (33), the κ_l are the eigenvalues (34) and $\phi_l(r)$ are the eigenfunctions of the spatial part of the operator in (26),

$$\left(\partial_r^2 + \frac{1}{r}\partial_r - \frac{(l-\mu(r))^2}{r^2} + 2\frac{\mu'(r)}{r}\right)\phi_l(r) = \kappa_l^2 \phi_l(r). \tag{34}$$

where, with (21),

$$\epsilon_{\mu\nu} \begin{pmatrix} 1 \\ i \\ 0 \\ 0 \end{pmatrix}_\nu = i \begin{pmatrix} 1 \\ i \\ 0 \\ 0 \end{pmatrix}_\mu \tag{35}$$

was used. In the mode decomposition (33), the coefficients $\psi_l(x_\alpha)$ are the free coefficients which, in the procedure of canonical quantization, become the operators. These $\psi_l(x_\alpha)$ are complex fields depending on two variables, x_3 and x_0 (or x_4 in a Euclidean version).

The eigenvalue problem (34), describing the tachyonic modes (33), has scattering solutions and bound state solutions as well. The scattering solutions have $\kappa_l = ik$ and, of course, a continuous spectrum. In contrast, the bound state solutions have real κ_l, are normalizable and have a discrete spectrum. In the following, we consider only these solutions. The methods for solving the eigenvalue problem (34) are well known. We demonstrate their application in Appendix A. There are no analytical formulas, but the numerical evaluation is quite easy using standard methods. We demonstrate the result in Figure 1 (left panel) as function of

$$\delta = \frac{BR^2}{2}, \tag{36}$$

which by means of $\delta = \Phi/2\pi$, is related to the magnetic flux (31). We mention that for $\delta < 0.08$ there is no solution, which is similar to the restriction $gB \leq p_3$, now in the

transversal direction. By increasing the flux, with each new flux quantum, one new solution comes down from the continuum. In the limit of $R \to \infty$, one will see all the degenerated solutions known from the homogeneous field. In Figure 1, in this limit all curves will merge into the dashed line. Spelled out in the reverse order, the finite extend of the magnetic field splits the tachyonic levels, i.e., it removes the degeneracy, and there is now a finite number of them. In Figure 1, the dependence of the maximal number l_{max} of orbital momenta for a given flux δ is shown. For large flux, $l_{max} \to \delta$ holds.

The next step is to set up a field theory for the tachyonic mode. With Equation (33) and (A1), we have a mode expansion for the tachyonic modes. Similar expansions could be set up for all other non-tachyonic modes as well. However, as said above, we restrict ourselves to the tachyonic modes. The reason is that the other modes are stable. A theory with only the tachyonic modes appears when inserting (33) into (17) and integrating over the transversal coordinates. We obtain

$$\tilde{\mathcal{L}} = \int dx_\perp \, \mathcal{L} \equiv \tilde{\mathcal{L}}_2 + \tilde{\mathcal{L}}_4 \tag{37}$$

with

$$\begin{aligned} \tilde{\mathcal{L}}_2 &= -\sum_{l=0}^{l_{max}} \psi_l^*(x_\alpha)\left(-\partial_\alpha^2 + m_l^2\right)\psi_l(x_\alpha), \\ \tilde{\mathcal{L}}_4 &= -\lambda\delta \sum_{l_1,\ldots,l_4 \le l_{max}} \delta_{l_1-l_2,l_3-l_4} N_4(l_i)\ \psi_{l_1}^*(x_\alpha)\psi_{l_2}(x_\alpha)\psi_{l_3}^*(x_\alpha)\psi_{l_4}(x_\alpha) \end{aligned} \tag{38}$$

and the coefficients are

$$\begin{aligned} m_l^2 &= -\kappa_l^2, \quad \lambda = \frac{g^2}{\pi}, \\ N_4(l_i) &= \int_0^\infty dr\, r\, \phi_{l_1}(r)\phi_{l_2}(r)\phi_{l_3}(r)\phi_{l_4}(r). \end{aligned} \tag{39}$$

All these quantities depend on the flux δ as a parameter. In these formulas, we have put $R = 1$. The dependence on R can be restored simply by dividing (37) by R^2.

The masses m_l are the (imaginary) masses of the tachyonic modes. The coefficients $N_4(l_i)$ in the quartic contribution depend on the flux δ and can be calculated by inserting (A1) into the lower line in (39). We mention that these are symmetric in the arguments l_i. Some examples are shown in Figure 2. The case of a homogeneous background can be obtained from $R \to \infty$ in (A1) and (39). In that case, the wave functions and the integration are explicit and result in

$$N_4^{hom}(l_i) = \frac{\Gamma(l_1 + l_3 + 1)}{2^{l_1+l_3}\sqrt{\Gamma(l_1+1)\Gamma(l_2+1)\Gamma(l_3+1)\Gamma(l_4+1)}}. \tag{40}$$

These are the dashed lines in Figure 2. In the limit $R \to \infty$, as can be seen in Appendix A, the exterior solution (A2) is exponentially small, and the limit is reached exponentially fast. This is also the speed in which the dashed lines are reached in the figure. However, because for a given l some solutions start at $\sim \delta$, there are δ contributions that are far from the homogeneous limit (40).

The Lagrangian (37) describes a theory with a finite number of complex fields in two dimensions with negative mass square, (39) and a dimensional coupling (λ, (39), is dimensionless and was introduced for convenience). The eigenvalues κ_l^2 in (39) and the factor $N_4(l_i)$ have dimension R^{-2} (when restoring R), and their magnitude depends on the magnetic background field $B(r)$, resp., using the specific background (30) on B. We remind that there is also the classical background (12) with the energy (31).

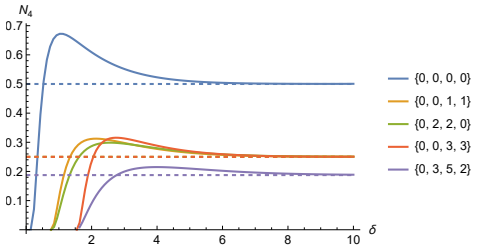

Figure 2. The coefficients $N_4(l_i)$ for sets $\{l_1, l_2, l_3, l_4\}$ from top to bottom: $\{0,0,0,0\}$, $\{0,0,1,1\}$, $\{0,2,2,0\}$, ...The dashed lines show the corresponding quantity in the case of a homogeneous background.

4. A Stable Tachyon Condensate

As discussed in [15], I assume that the tachyonic modes will form a condensate similar to the scalar field in the well-known Higgs model. With (37), we have a system with a kind of *Mexican hat potential* for the fields $\psi_l(x_\alpha)$. The negative mass square in $\tilde{\mathcal{L}}_2$ leads to the system for $\psi_l(x_\alpha) = 0$ to result in 'sitting on the top of the hill' and causes the effective potential to have an imaginary part, which is just that which was observed in [3] for a homogeneous background. In the preceding section, we have seen that these instabilities appear in the inhomogeneous background (30) as well. The imaginary part makes the system unstable and pushes it forwards to a state with lower energy until the imaginary part disappears. There are probably many ways for QCD to go to a lower state. Here, we consider those that are within the model defined by the Lagrangian (37). Thus, the system will create modes of the field $\psi_{l_1}(x_\alpha)$, i.e., tachyons, until it is stopped by the repulsive self-interaction given by $\tilde{\mathcal{L}}_4$ in (38). These modes will form a Bose condensate. The situation is similar to a quartic oscillator in quantum mechanics with an imaginary frequency and a x^4-term entering with a plus sign. So, we have to look for the minimum of the potential $-\tilde{\mathcal{L}}$. We mention that the existence of a minimum is guaranteed by the structure of $\tilde{\mathcal{L}}$ as all coefficients in $\tilde{\mathcal{L}}_4$, (38), are positive.

In [15], only one orbital momentum mode, $l = 0$, was allowed, and the above idea was realized by a shift, $\psi(x_\alpha) \to \psi(x_\alpha) + v$, of this mode, where v is a constant condensate. In the present case, we allow for all orbital momentum modes in (33) and have a correspondingly more complicated situation. As said above, we have to consider the minimum of $-\tilde{\mathcal{L}}$, (37). In view of a later quantization, this means that we consider a minimum of the effective potential (which would include quantum corrections) on the tree level.

We parameterize the complex fields,

$$\psi_l(x_\alpha) = \frac{1}{\sqrt{2}} \varphi_l(x_\alpha)\, e^{i\Theta_l(x_\alpha)} \tag{41}$$

by two real fields, $\varphi_l(x_\alpha)$ and $\Theta_l(x_\alpha)$, having a meaning of module and phase. We mention that $\tilde{\mathcal{L}}_4$ in (38) is real, which is ensured by the Kronecker symbol in (38), i.e., by the orbital momentum conservation.

In the following, we look for a minimum on constant fields. An inhomogeneity only tends to increase the energy. Of course, a minimum on non-constant fields cannot be excluded in such simple way. However, this is a separate problem and is left for later. Because there is no way to obtain analytical results, we are left with numerical methods. The calculations were preformed using Mathematica with the tools provided by that system.

To look for a minimum, we make shifts of the fields,

$$\varphi_l(x_\alpha) \to v_l + \varphi_l(x_\alpha), \quad \Theta_l(x_\alpha) \to \vartheta_l + \Theta_l(x_\alpha) \tag{42}$$

with constant v_l and ϑ_l.

We insert (41) and (42) into the Lagrangian (37) and expand for small $\varphi_l(x_\alpha)$ and $\Theta_l(x_\alpha)$. We arrive at

$$\hat{\mathcal{L}} = \hat{\mathcal{L}}_0 + \hat{\mathcal{L}}_1 + \hat{\mathcal{L}}_2 + \dots \tag{43}$$

with

$$\begin{aligned}
\hat{\mathcal{L}}_0 &= \frac{1}{2}\sum_{l=0}^{l_{max}} \kappa_l^2 v_l^2 - \frac{g^2}{2\pi}\delta \sum_{l_1,\dots,l_4\le l_{max}} \delta_{l_1-l_2,l_3-l_4} N_4(l_i)\; v_{l_1} v_{l_2} v_{l_3} v_{l_4}\; e^{i\vartheta_{l1}-i\vartheta_{l2}+i\vartheta_{l3}-i\vartheta_{l4}}, \qquad (44)\\
\hat{\mathcal{L}}_1 &= \sum_{l=0}^{l_{max}} \left[\kappa_l^2 v_l - 4\frac{g^2}{2\pi}\delta \sum_{l_1,\dots,l_4\le l_{max}} \delta_{l_1-l_2,l_3-l_4} N_4(l_i)\; \delta_{l,l_1} v_{l_2} v_{l_3} v_{l_4}\right]\varphi_l(x_\alpha),\\
\hat{\mathcal{L}}_2 &= -\sum_{l=0}^{l_{max}} \left[\frac{1}{2}\varphi_l(x_\alpha)\left(-\partial_\alpha^2\delta_{ll'} + m_{ll'}^2\right)\varphi_l(x_\alpha) + v_l^2\Theta_l(x_\alpha)(-\partial_\alpha^2)\Theta_l(x_\alpha)\right].
\end{aligned}$$

The mass is now a matrix with entries

$$m_{ll'}^2 = -\kappa_l^2\delta_{ll'} + 3\frac{g^2}{2\pi}\delta \sum_{l_1,\dots,l_4\le l_{max}} \delta_{l_1-l_2,l_3-l_4} N_4(l_i)\delta_{l,l_1}\delta_{l,l_2}\; v_{l_3} v_{l_4}. \tag{45}$$

We are looking for a minimum of $\hat{\mathcal{L}}_0$, which at once is a zero of $\hat{\mathcal{L}}_1$. We mention that the $\vartheta_l(x_\alpha)$ do not cancel in $\hat{\mathcal{L}}_0$. The first appearance of a ϑ_l is for $\delta = 3.03$, where we have orbital momenta until $l = 3$,

$$\begin{aligned}
\hat{\mathcal{L}}_0 = {} & -2.89926v_0^2 - 2.46514v_1^2 - 1.67909v_2^2 - 0.640937v_3^2 \qquad (46)\\
& + \lambda\big[0.218062v_1^2v_2v_0\cos(\vartheta_0 - 2\vartheta_1 + \vartheta_2) + 0.256459v_1v_2v_3v_0\cos(\vartheta_0 - \vartheta_1 - \vartheta_2 + \vartheta_3)\\
& + 0.158381v_1v_2^2v_3\cos(\vartheta_1 - 2\vartheta_2 + \vartheta_3) + 0.137526v_0^4 + 0.296608v_1^2v_0^2 + 0.161249v_2^2v_0^2 + 0.0745899v_3^2v_0^2\\
& + 0.0737236v_1^4 + 0.0502424v_2^4 + 0.0234354v_3^4 + 0.220456v_1^2v_2^2 + 0.124823v_1^2v_3^2 + 0.130519v_2^2v_3^2\big],
\end{aligned}$$

to show an example.

It is worth mentioning that the minimum may be not unique. In the example (46), a change in the angles ϑ_i, keeping the arguments of the cosines, is possible as that would imply three conditions for four variables. In the following, we consider only one minimum. As it turned out, one of them is realized for all $\vartheta_l = 0$. For this reason, we dropped the ϑ_l in $\hat{\mathcal{L}}_1$. In (44), the last line is the quadratic part of the Lagrangian. It is not non-diagonal in the fields $\varphi_l(x_\alpha)$. The fields $\Theta_l(x_\alpha)$ remain massless, and in the sense of a spontaneous symmetry, breaking these are the Goldstone bosons. In this spirit, we call the v_l, which realize the minimum of $\hat{\mathcal{L}}_1$, the *tree-level condensates* v_l^{tree} and the value of $\hat{\mathcal{L}}_0$,

$$V_{eff}^{tree} \equiv -\hat{\mathcal{L}}_0\big|_{v_l^{tree}}, \tag{47}$$

the effective potential on tree level.

Some of the first (in the sense of increasing flux δ) condensates and V_{eff}^{tree} are shown in Figure 3 (right panel) for $\delta \le 4$. The depth of the minimum of V_{eff}^{tree} grows with the flux. Until $\delta = 3.03$, we have only one non-zero condensate, v_1^{tree}; beyond this, all components may be non-zero.

The behavior of the condensates deserves special attention. Until $\delta = 3.03$, we have up to four orbital momentum modes present (see Figure 1) and only one non-zero condensate. At $\delta = 3.03$, without exciting a new orbital mode, the behavior changes drastically; now, all condensates v_l ($l = 0, \dots, 3$) are non-zero (see Figure 3, right panel). At $\delta = 3.25$, the mode $l = 4$ sets in, and here we have each second condensate as non-zero. We did not investigate this behavior in more detail, but we assume that classical chaos can be observed here.

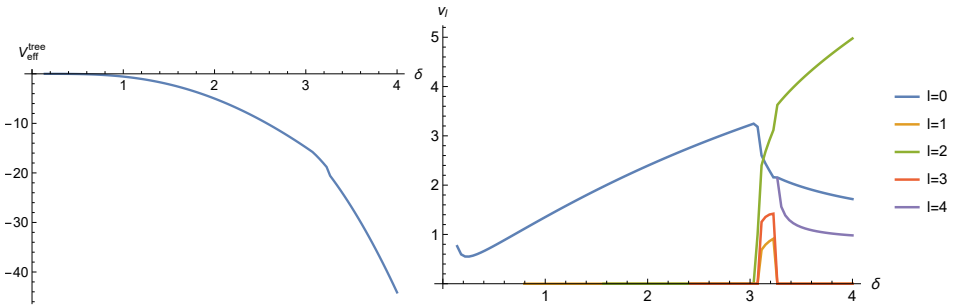

Figure 3. Left panel: The value of $V_{eff}^{tree} = -\mathcal{L}$, (37), in the minimum. **Right panel**: The tree level condensates v_l^{tree} as a function of the flux δ. The mesh for these plots is $\Delta\delta = 0.039$.

In the minimum of V_{eff}^{tree}, the first-order variation in $\varphi_l(x_\alpha)$, i.e., $\hat{\mathcal{L}}_1$, vanishes. This circumstance was used in the numerical calculations as a check for the procedure to find the minimum. For instance, the expression

$$\sum_{l=0}^{l_m} \Big| -\kappa_l^2 (v_l^{tree})^2 + \lambda\delta \sum_{l_i} \delta_{l,l_1} N_4(l_i) \delta_{l_1-l_2,l_3-l_4} v_{l_1}^{tree} v_{l_2}^{tree} v_{l_3}^{tree} v_{l_4}^{tree} \Big|, \tag{48}$$

which accumulates the mismatches from the first variations, was seen to be below 10^{-9} for all calculated values of δ. In order to reach this, in the integration in (39), in the routines for finding the minima of $-\mathcal{L}$ and for solving Equation (A8) for κ_l, a working precision of 100 digits was used.

In the second-order variation, $\hat{\mathcal{L}}_2$, we have a mass matrix, (45). It can be diagonalized, and the eigenvalues are shown in Figure 4 (and in Figure 5 for larger δ). These are all non-negative and grow with the flux.

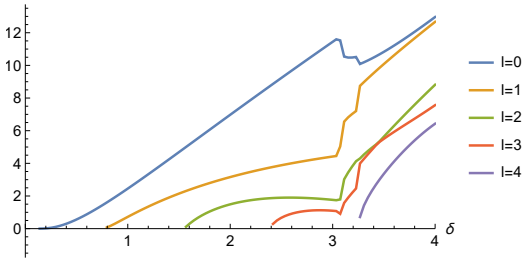

Figure 4. The mass eigenvalues on the tree level, i.e., after diagonalization of (46).

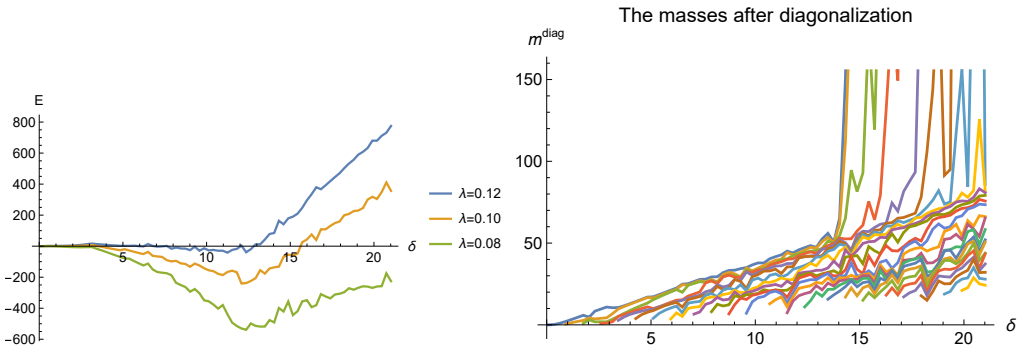

Figure 5. Left panel: The energy E, (47), of the system. **Right panel**: The mass eigenvalues on the tree level, i.e., after diagonalization of (46), for $\lambda = 0.1$. The mesh for these plots is $\Delta\delta = 0.28$.

As can be also observed from these figures, after $\delta = 3.03$, the behavior becomes a bit irregular (similar to that of the condensates in Figure 3); however, it keeps its basic features.

The same holds for the energy in Figure 5 (left panel). The unevenness of the curve is not due to numerical errors but is an intrinsic property.

The minimum of the complete energy, i.e., with the energy (12), or (31), with the background field added, is

$$E = E_{bg} + V_{eff}^{tree} \tag{49}$$

with $\mathcal{L}$ being from (37) and v_l^{tree} being inserted. Restoring the R dependence, a factor R^{-2} must be added. As a function of δ, the energy E is shown in Figure 5 (left panel) for several values of the coupling λ. As can be seen, for large λ, there is no minimum. It appears at $\lambda \sim 0.12$ and deepens with decreasing λ. In the right panel of Figure 5, m^{diag}, i.e., the eigenvalues of the mass matrix (45), are shown. This is a continuation of Figure 4 to larger δ. All of these masses are positive, and some become large.

It is interesting to mention that the effective potential (47), which is shown in Figure 3 for small δ, continues to also grow in the negative direction for larger δ, as shown in Figure 6 in comparison with the energy E, (49).

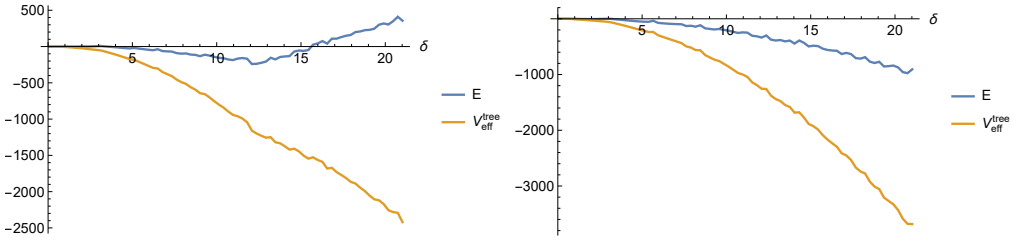

Figure 6. Left panel: The effective potential (47) and energy (49) for $\lambda = 0.1$. **Right panel**: The effective potential (47) and energy (49) for $\lambda = 0.1$ calculated with N_4^{hom}, (40), in place of N_4, (39).

Now, let us discuss the relation to a homogeneous magnetic background. Formally, it corresponds to an infinite radius in our model, $R \to \infty$. Of course, the energy diverges as being proportional to the area in the directions perpendicular to the magnetic field. Equivalently, in the radial gauge, the number of orbital momenta involved diverges. Therefore a regularization is needed. As such, just the finite radius, which is considered in this paper, may be taken. For instance, it provides a restriction for the orbital momenta, l_{max}; see Figure 1. Considering R, or l_{max}, as regularization, we have the same formulas as before with the only change being that we may take N_4^{hom}, (40), in place of N_4, (39). The result is shown in Figure 6 in the right panel. Both the effective potential and the energy are below the corresponding values in the left panel and, in addition, the energy has a non-minimum. This behavior demonstrates for instance that taking a restriction of the angular momenta as regularization for a calculation in the homogeneous background gives wrong results.

5. Discussion and Conclusions

In the preceding section, we have seen that in a string-like chromomagnetic background, the tachyonic modes of the gluon field will form a condensate. We took for the background a homogeneous field inside a cylinder of radius R and a zero field outside. It has a finite flux Φ and a finite energy E_{bg} (per unit length of the cylinder), (31). Due to the cylindrical symmetry, we have orbital modes of the tachyon field, $\psi_l(a_\alpha)$, (33). Their number is restricted by the flux, $0 \le l \lesssim \delta$ (see Figure 1, right panel). Each orbital momentum mode may have a condensate, whereby we considered only constant condensates of the module $\varphi_l(a_\alpha)$, (41).

To find the minimum of $-\mathcal{L}_0$, (44), is a task in several variables. We used the numerical capabilities provided by Mathematica. The depth of the emerging minimum is shown in Figure 3 (left panel) and for larger δ in Figure 6 (also left panel, upper curve) as a function of the flux δ. It takes negative values and grows with the flux.

An unexpected feature is the structure of the minima for $\delta > 3.03$. As can be seen in Figure 3 (right panel) and also in Figure 4, the behavior of the solutions changes drastically; however, they keep the basic features. We interpret this phenomenon as the onset of classical chaos.

The minimum V_{min} of the effective potential V_{eff}^{tree}, (47), deepens with growing flux. To obtain the total energy, one has to add the energy of the background field E_{bg}, (31). Using (36), one comes to (49). Restoring the R dependence, it can be written in the form

$$E = \frac{\pi\delta + V_{min}}{R^2}. \tag{50}$$

As can be seen from Figure 5 (left panel), for a coupling $\lambda \lesssim 0.12$, it has a minimum at some finite δ. With fixed radius R, the corresponding value of the magnetic field would be chosen by the system automatically.

In case one also allows the radius to be a dynamical variable, the system would prefer $R \to 0$ as the direction lowering the energy. We mention that this is a result of our purely classical consideration. We may hope that this shrinking of the radius will be stopped when quantum effects are included.

We started from SU(2) chromodynamics. We separated the tachyonic modes and have seen that these will create a chromomagnetic background field and will form a stable condensate. It is worth mentioning that this approach is in distinction from the most common assumption of the condensate for all gluon modes, which is motivated by keeping the gauge symmetry. An attractive feature of our approach is that a condensate of the tachyon modes provides masses to all these modes; see Figure 5 (right panel). This is similar to the Higgs mechanism in the Standard Model.

A task for further investigation in this approach is the calculation of the vacuum energy of the tachyonic modes. Because all of these have real, non-zero masses (see Figure 5 (right panel), this should not be a problem. Moreover, when including temperature, a simple estimation for high T, following Equation (49) in [15], shows that additional contributions $\sim \sum_l m_l T$ can be expected, removing any minimum and restoring the initial symmetry.

A further development must be the inclusion of the non-tachyonic modes. Here, one may encounter the problem where the considered magnetic string is not a solution of the initial equations of motion as $\mathcal{L}_1$, (25), is not zero. As long as the consideration is restricted to the tachyonic modes, this is not a problem, as $\mathcal{L}_1$ couples only to the third color component.

Funding: This research received no external funding.

Data Availability Statement: No new data were created or analyzed in this study. Data sharing is not applicable to this article.

Conflicts of Interest: The authors declare no conflicts of interest.

Appendix A. Bound State Solutions in the Flux Tube

In this appendix, we demonstrate the solution of the eigenvalue problem (34) and follow standard methods. The problem can be viewed as a stationary Schrödinger equation. It has discrete eigenvalues with $\kappa_l^2 > 0$ and scattering states with $\kappa_l^2 < 0$. The bound state solutions, which correspond to the tachyonic modes, must decrease for $r \to \infty$. The solutions can be found in terms of the Bessel function in the outside region and in terms of the Kummer functions in the inside region,

$$\phi_l(r) = \frac{1}{N_l}\Big(\phi_l^{\rm int}(r)\Theta(R-r) + \phi_l^{\rm ext}(r)\Theta(r-R)\Big), \tag{A1}$$

matching functions and their derivatives by continuity at $r = R$. In this way, for the outside function, we make the ansatz

$$\phi_l^{\rm ext}(r) = \beta_l K_\nu(\kappa r) \tag{A2}$$

where β_l are some constants, $\nu = l - \frac{BR^2}{2}$, $K_\nu(\kappa r)$ is a modified Bessel function, and κ is still to be found. To find the inside function $\phi_l^{\rm int}(r)$, we follow a well-known procedure and make a substitution

$$\rho = \frac{Br^2}{2}, \tag{A3}$$

of the radial variable and the ansatz

$$\phi_l^{\rm int}(r) = \rho^{l/2} e^{-\rho/2} M(\rho). \tag{A4}$$

Equation (34) turns into

$$\left(\rho\partial_\rho + (l+1-\rho)\partial_\rho - \frac{R^2}{2\delta} - l + \frac{1}{2}\right) M(\rho) = 0, \tag{A5}$$

where we use the notation $\delta = BR^2/2$, (32).

The solution of Equation (A4), which is regular at the origin, is the Kummer function $M(a, l+1, \rho)$ with the notation

$$a = \frac{\kappa^2 R^2}{2\delta} + l - \frac{1}{2}. \tag{A6}$$

In order to find the eigenvalues, it is sufficient to match the logarithmic derivatives. For this, we define

$$R^{\rm ext}(r) = \kappa\partial_r \ln \phi_l^{\rm ext}(r), \quad R^{\rm int}(r) = \kappa\partial_r \ln \phi_l^{\rm int}(r) \tag{A7}$$

and demand

$$R^{\rm ext}(R) = R^{\rm int}(R). \tag{A8}$$

It is convenient to introduce another dimensionless notation, $x = \kappa R$, and to rewrite

$$\begin{aligned} R^{\rm ext}(R) &= x\partial_x \ln K_\nu(x), \\ R^{\rm int}(R) &= l - \delta + \frac{2\delta a}{l+1} \frac{M(a+1, l+2, \delta)}{M(a, l+1, \delta)} \end{aligned} \tag{A9}$$

where Equation (9.213) from [16] was used.

The solutions κ_l of Equation (A8) are the eigenvalues of the operator on the left side of (34). The coefficients β_l and the normalization factors N_l in Equation (A1) can be found from matching the functions and from

$$\int_0^\infty dr\, r\, \phi_l(r)\phi_{l'}(r) = \delta_{ll'}, \tag{A10}$$

which is the normalization condition.

References

1. Eichhorn, A.; Gies, H.; Pawlowski, J.M. Gluon condensation and scaling exponents for the propagators in Yang-Mills theory. *Phys. Rev. D* **2011**, *83*, 045014. [CrossRef]
2. Savvidy, G.K. Infrared instability of vacuum state of gauge theories and asymptotic freedom. *Phys. Lett. B* **1977**, *71*, 133–134. [CrossRef]
3. Nielsen, N.K.; Olesen, P. Unstable Yang-Mills Field Mode. *Nucl. Phys. B* **1978**, *144*, 376–396. [CrossRef]

4. Nielsen, H.B.; Olesen, P. A quantum liquid model for the QCD vacuum: Gauge and rotational invariance of domained and quantized homogeneous color fields. *Nucl. Phys. B* **1979**, *160*, 380–396. [CrossRef]
5. Flory, C.A. Covariant Constant Chromomagnetic Fields and Elimination of the One Loop Instabilities. Preprint, SLAC-PUB3244. 1983. Available online: http://wwwpublic.slac.stanford.edu/sciDoc/docMeta.aspx (accessed on 1 January 2024).
6. Leutwyler, H. Vacuum Fluctuations Surrounding Soft Gluon Fields. *Phys. Lett.* **1980**, *96*, 154–158. [CrossRef]
7. Savvidy, G. Stability of Yang Mills vacuum state. *Nucl. Phys. B* **2023**, *990*, 116187. [CrossRef]
8. Skalozub, V.; Bordag, M. Color ferromagnetic vacuum state at finite temperature. *Nucl. Phys. B* **2000**, *576*, 430–440. [CrossRef]
9. Dittrich, W.; Schanbacher, V. The effective QCD lagrangian at finite temperature. *Phys. Lett. B* **1981**, *100*, 415–419. [CrossRef]
10. Vercauteren, D.; Verschelde, H. Resolving the instability of the savvidy vacuum by dynamical gluon mass. *Phys. Lett. B* **2008**, *660*, 432–438. [CrossRef]
11. Kondo, K.I. Stability of chromomagnetic condensation and mass generation for confinement in SU(2) Yang-Mills theory. *Phys. Rev. D* **2014**, *89*, 105013. [CrossRef]
12. Nedelko, S.; Voronin, V. Energy-driven disorder in mean field qcd. *Phys. Rev. D* **2021**, *103*, 114021. [CrossRef]
13. Diakonov, D.; Maul, M. Center-vortex solutions of the Yang-Mills effective action in three and four dimensions. *Phys. Rev. D* **2002**, *66*, 096004. [CrossRef]
14. Bordag, M. Vacuum energy of a color magnetic vortex. *Phys. Rev.* **2003**, *D67*, 065001. [CrossRef]
15. Bordag, M. Tachyon condensation in a chromomagnetic background field and the groundstate of QCD. *Eur. Phys. J. A* **2023**, *59*, 55. [CrossRef]
16. Gradshteyn, I.S.; Ryzhik, I.M. *Table of Integrals, Series and Products*; Academic Press: New York, NY, USA, 2007.